Signal Processing and Renewable Energy
June 2020, (pp. 1-22)
ISSN: 2588-7327
eISSN: 2588-7335

MPPT and Current Mode Control Methods for PV Modules: A Review and A New Multi-Loop Integrated Method

Ali Moghassemi[1], Shayan Ebrahimi[1], Javad Olamaei[1*]

[1] Department of Electrical Engineering, South Tehran Branch, Islamic Azad University, Tehran, Iran.

Received: 29-Sep-2019, Revised: 16-Dec-2019, Accepted: 22-Dec-2019.

Abstract

This paper reviews various algorithms for the implementation of MPPT in a PV module integrated with a DC-DC converter and current mode control strategies for power converters. Also, a novel multi-loop integrated MPPT and current mode control for the Single Ended Primary Inductance Converter (SEPIC) derived from the incremental conductance MPPT technique is proposed. A simulation model is developed using MATLAB/Simulink dynamic system simulation software to verify the operation of the control system developed in the paper. This ensures the efficient operation of the PV power plant by rapid and accurate tracking the maximum power point (MPP) of the PV array. Moreover, the system is seen to offer robust voltage regulation and improved dynamic response in the face of changing environmental variables.

Keywords: MPPT, PV Module, Current Mode Control, Incremental Conductance Method.

1. INTRODUCTION

Solar energy is clean, inexhaustible and free as one of the most important renewable energy. The application of photovoltaic (PV) system becomes more and more widely, the main application of PV systems is in either stand-alone or grid-connected configurations. Solar PV generation is an important form of solar energy utilization, it is one of the most promising power generation technologies due to restrictions from raw materials and application environment. There are two major technical difficulties of PV generation systems in the application. Firstly, the conversion efficiency of electric power generation is low. Generally, laboratory cell efficiency is approximately 18–20% and the commercial cell efficiency is about 13–18%; Secondly,

*Corresponding Authors Email: j_olamaei@azad.ac.ir

the output power of PV cells is influenced by the radiance and ambient temperature. To overcome these problems, we should track the maximum power point of the PV cells' output power. Thus, this improves the efficiency of the PV power generation system, reducing the cost of power generation.

The power output of any PV module is a function of environmental variables like insolation (incident solar radiation), temperature, shading (from trees and cloud cover) and load conditions [1]. However, insolation and temperature conditions are the prime variables. Thus, the current-voltage (I-V) characteristics and the power-voltage (P-V) characteristics of solar modules are affected by the insolation and temperature levels. The output current and hence the output power increase linearly with insolation while the output voltage and hence the output power decreases with increasing temperature. These two environmental variables change constantly throughout the day and consequently give rise to the intermittency and variability associated with the production of energy by solar modules. However, the PV module has a single operating point where the values of the current and voltage of the module result in a maximum power output [1-3].

Figures 1 and 2 show such an operating point for the I-V characteristics and P-V characteristics. As it is seen in the Figures, such a maximum power point (MPP) occurs at the knee of the curve. At this point, the module delivers the maximum power from the source to its load [3]. Ensuring that the PV module operates at this desired MPP and hence at the highest efficiency, requires a robust control strategy to track this ever-changing point [4, 5].

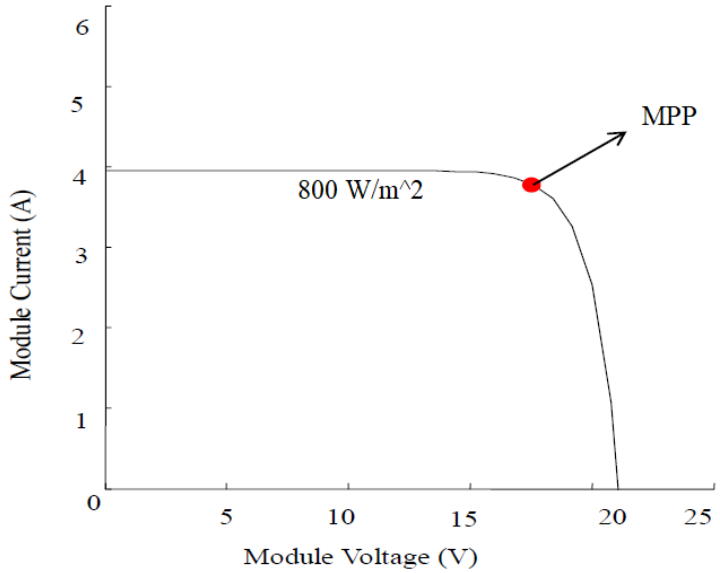

Fig. 1. The I-V curve of a PV module showing the MPP at 800 W/m^2.

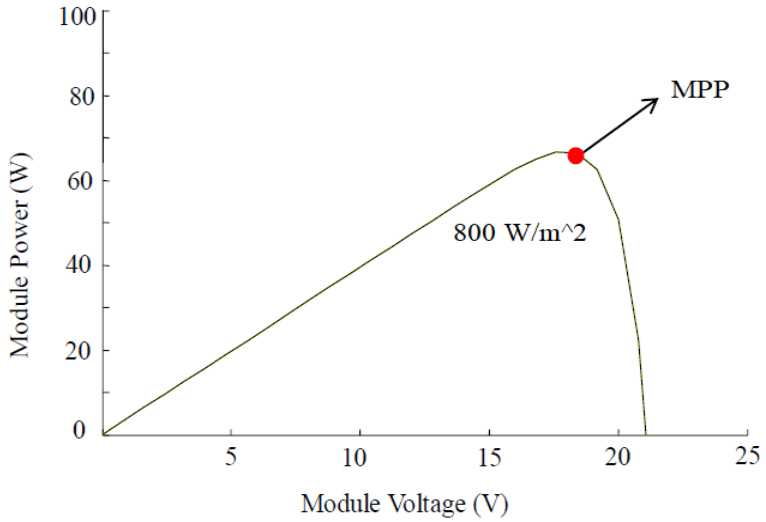

Fig. 2. The P-V curve of a PV module showing the MPP at 800 W/m^2.

This tracking task is often implemented using maximum power point tracking (MPPT) control algorithm-several of which exist in the literature [6, 7]. The extraction of this maximum power is often done in conjunction with a power conditioning unit (DC-DC or DC-AC converters) as the interface between the PV modules and the system electrical load [1, 8]. Such a power conditioning unit, in addition to ensuring operation at the MPP, must also ensure the regulation of the output voltage and current irrespective of load and input voltage variations.

This paper discusses these two control approaches that ensure that the SEPIC converter-based PV power system operates: 1) efficiently by extracting the maximum available power from the PV module and, 2) offers robust regulation of the output voltage and the current using the current-mode technique. Firstly, a review of the existing MPPT techniques is carried out, highlighting the pros and cons of each approach. This is followed by a review of some current-mode control methodologies. Thirdly, a robust multi-loop control system incorporating the MPPT and current-mode control are proposed and used to control the SEPIC converter and the PV array output. Finally, the performance of the proposed control system is studied via simulations using the simulation model developed in the MATLAB/Simulink software.

2. REVIEW OF MPPT ALGORITHMS

2.1. Perturb and Observe (P&O) Technique

The P&O technique [10-13] is the most commonly used MPPT tracking algorithm because of its ease of implementation. It is based on a hill-climbing approach to the maximum power point of the power-voltage characteristics of the PV module as illustrated in Figure 3. It uses the fact that the slope of such a curve is zero at the MPP, positive on the left-hand side of the MPP (increasing power zone), and negative on the right-hand side of the MPP (decreasing

power zone) [10-13]. This is explained mathematically by equations (2-4) [12, 13].

$$\frac{dP}{dV} = \frac{d(V \times I)}{dV} = V \times \frac{dI}{dV} + I \quad (1)$$

$$\frac{dP}{dV} = 0 \Rightarrow \frac{I}{V} = \frac{-dI}{dV} \Rightarrow at\ the\ MPP \quad (2)$$

$$\frac{dP}{dV} > 0 \Rightarrow \frac{I}{V} > \frac{-dI}{dV} \Rightarrow left\ of\ the\ MPP \quad (3)$$

$$\frac{dP}{dV} < 0 \Rightarrow \frac{I}{V} < \frac{-dI}{dV} \Rightarrow right\ of\ the\ MPP \quad (4)$$

The operating criterion of this algorithm is based on the perturbation (increase or decrease) of the solar PV module variable of interest-either voltage or current. If the variable (voltage) is perturbed in a given direction, the algorithm checks for a corresponding increase or decrease in the array power by comparing it with that of the previous perturbation cycle. If an increase is detected, it means the operating point is on the left side of the MPP and therefore the operating voltage must be further perturbed in the same direction. Otherwise, for power decrease, the operating point is on the right side of MPP and therefore operating voltage must be perturbed in the reverse direction. This iterative process is repeated until the MPP is tracked. The flowchart of the algorithm is illustrated in Figure 4.

The P&O technique offers the following advantages [11, 12]: 1) ease of implementation; 2) low cost of implementation. The disadvantages include: [11-13]: 1) energy losses arising from the oscillation of operating point around the MPP at steady-state operation; 2) in rapidly changing atmospheric conditions, the P&O algorithm performance becomes very questionable since it exhibits a slow dynamic response; 3) slow tracking speed.

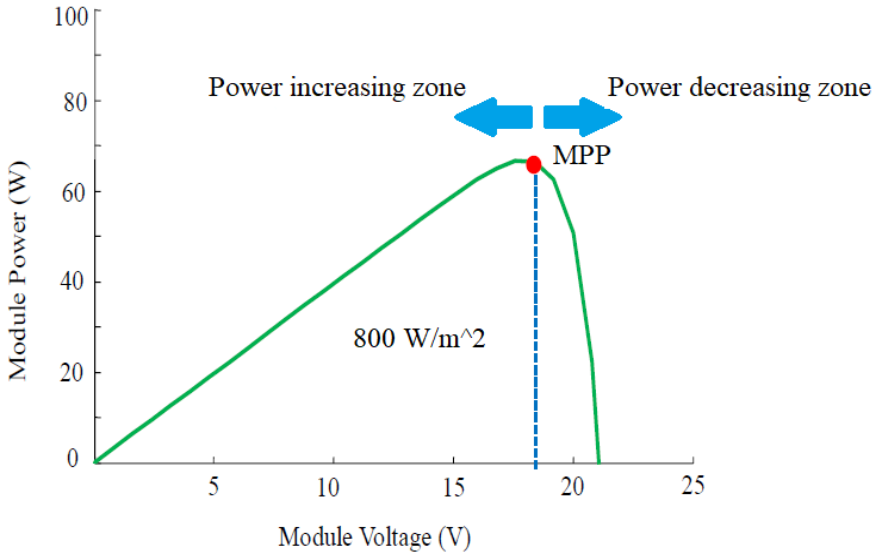

Fig. 3. Illustration of the P&O MPPT technique.

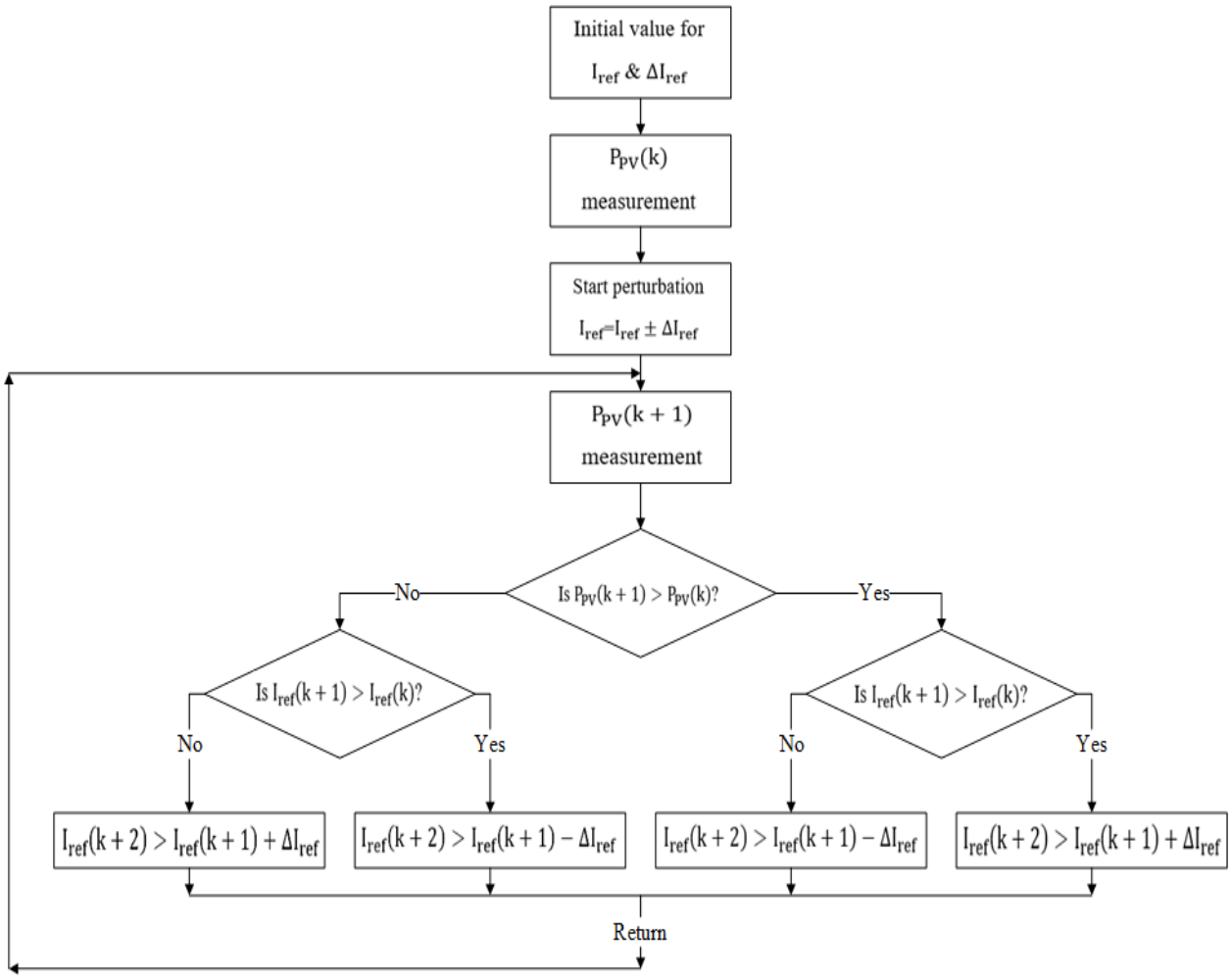

Fig. 4. Flowchart of conventional P&O algorithm.

2.2. Improved Versions of the P&O Technique

Many variations of the conventional P&O technique described above exist in the literature [11]. These variations attempt to overcome the shortcomings of conventional P&O and improve performance. These modified techniques often involve: 1) using variable step size instead of fixed step size for perturbation. This is the so-called Adaptive P&O technique [10]; 2) the use of larger or smaller a fixed step size of the perturbation. Larger values cause oscillation while smaller values result in slow response [2]. Thus, the need for an effective trade-off between fast response and oscillation often arises; 3) utilization of the converter duty ratio as the perturbation signal instead of using the array voltage or current [10, 12].

2.3. Incremental Conductance (I&C) Technique

The I&C Technique is based on the fact that the MPP can be tracked accurately by comparing the incremental conductance ($\Delta I / \Delta V$) with the instantaneous conductance

(I/V) of the PV array [14-20]. The sum of these two values is zero at MPP, negative on the right side of MPP and positive on the left side of MPP as shown in Figure 5. Thus, the algorithm searches for the MPP using equations (5-7). That is, if the operating point is to the left of MPP, (5) increases the control variable and hence the duty cycle.

$$\frac{\Delta I}{\Delta V} > -\frac{I}{V} \quad (5)$$

Similarly, if the operating point is to the right of MPP, (6) decreases the control variable and hence the duty cycle.

$$\frac{\Delta I}{\Delta V} < -\frac{I}{V} \quad (6)$$

And when the operating point is at MPP, equation (7)keep the previous value of the variable and hence the duty cycle.

$$\frac{\Delta I}{\Delta V} = -\frac{I}{V} \quad (7)$$

The detailed operation of the algorithm is explained with the help of the flowchart in Figure 6. The algorithm starts its iterative process by obtaining the input voltage $V(t)$, and current $I(t)$, from the panel. These values are compared with values at the end of the preceding cycle $V(t-1)$ and $I(t-1)$. Thus, the incremental change is [15]:

$$\Delta V = V(t) - V(t-1) \quad (8)$$

The next step in the cycle is the checking of the conditions given (equations (5-7)) as explained before. In practice, it is difficult to satisfy equation (7) due to noise and errors and hence the condition is modified with good approximation by [5]:

$$\left|\frac{\Delta I}{\Delta V} + \frac{I}{V}\right| < \varepsilon \quad (9)$$

where, ε is a positive small value. The I&C algorithm has the following advantages [14-17]: 1) high accuracy in tracking the MPP in rapidly changing environmental conditions; 2) medium implementation complexity. The disadvantages of the method include [18-20]: 1) increased hardware and software complexity when compared to the P&O algorithm; 2) increased computational time occasioned by the complexity of the hardware.

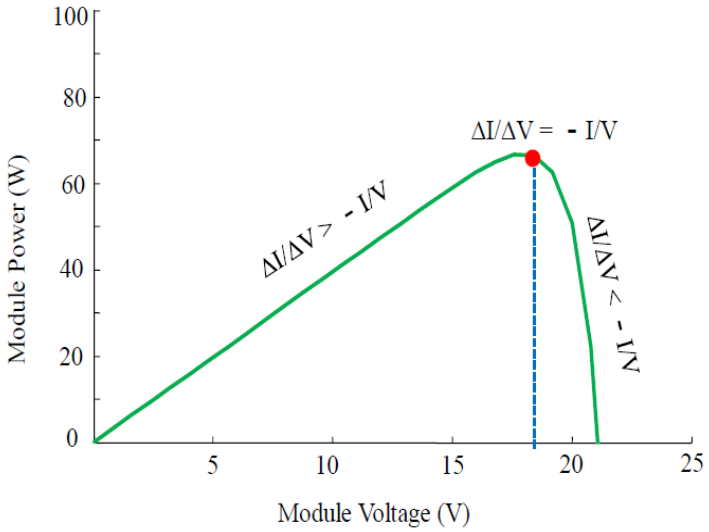

Fig. 5. P-V curve of a PV array showing the three regions of the I&C algorithm.

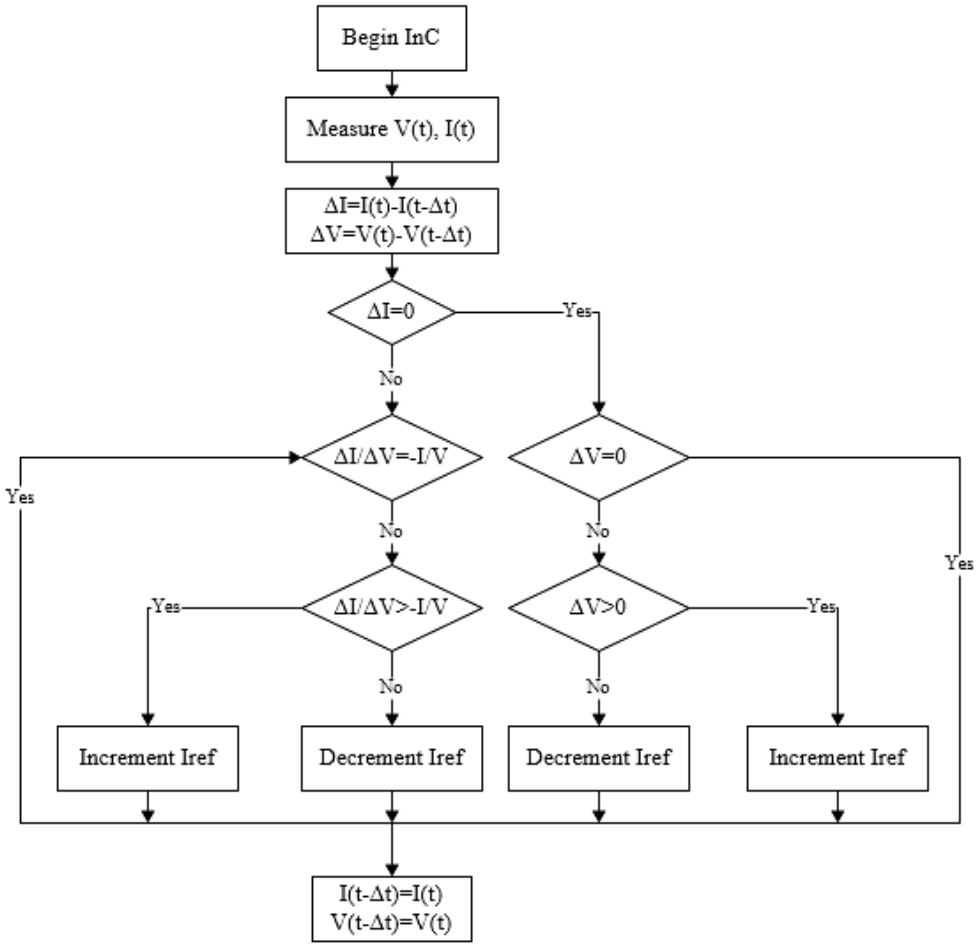

Fig. 6. Flowchart of I&C algorithm.

2.4. Ripple Correlation Control (RCC) Technique

The switching actions of power converters (whether DC-DC or DC-AC) result in the generation of current and voltage ripples. These ripples are usually injected into the PV array line. The RCC technique uses these ripples to extract information about the power gradient and evaluate if the PV system operates close to the maximum power point [21]. Thus, the RCC technique finds the correlation between the time derivative of the time-varying PV power and the time derivative of the time-varying array current or voltage. For a PV power curve (P-V characteristics) the RCC technique is explained by the following relationships [21, 22]:

$$\frac{dP}{dt} \times \frac{dV}{dt} > 0 \Rightarrow V_{pv} < V_{mp} \tag{10}$$

$$\frac{dP}{dt} \times \frac{dV}{dt} < 0 \Rightarrow V_{pv} > V_{mp} \tag{11}$$

$$\frac{dP}{dt} \times \frac{dV}{dt} = 0 \Rightarrow V_{pv} = V_{mp} \tag{12}$$

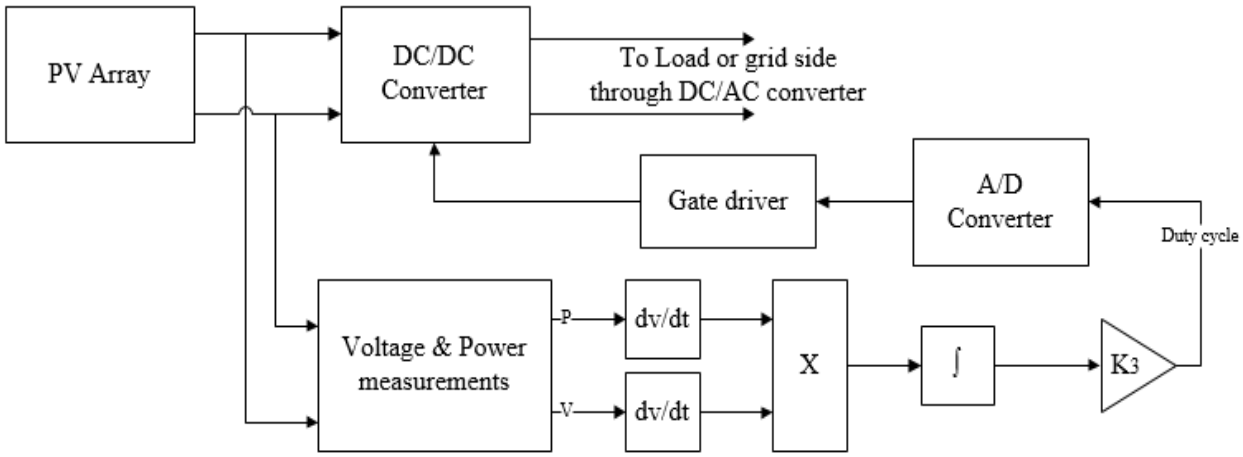

Fig. 7. Implementation of RCC-based MPPT technique.

where, V_{pv} is the operating voltage and V_{mp} is the voltage at the MPP. Equation (10) shows that the operating point will be below (to the left side) the MPP if the ripple voltage or the ripple current and the power both increases. Similarly, equation (11) shows that the operating point will be above (to the right side) the MPP if the ripple current or voltage increases while the power decreases. Equation (12) locates the MPP. Thus, it is seen that the phase relationship between the power ripple and the array voltage or current decides the tracking direction and the associated change in the duty ratio. Controlling the duty ratio of the converter based on the relationship in equations (13-14) continuously tracks the MPP [21, 23].

$$dt = -K \int \frac{dP}{dt} \times \frac{dV}{dt} dt \qquad (13)$$

$$dt = K \int \frac{dP}{dt} \times \frac{dI}{dt} dt \qquad (14)$$

where, d is the duty ratio of the converter and K is a positive constant. Figure 7 is an illustration of the implementation of the RCC MPPT technique. The RCC technique has the following advantages [21-24]: 1) Since the technique is PV array independent, implementation is easy. That is, it yields parameter-insensitive MPPT of the PV system; 2) it offers fast-tracking speed even under rapid changing environmental conditions; 3) low cost of implementation. However, the RCC technique has the following disadvantages: 1) the technique offers low accuracy; 2) unsuitable for high switching frequency.

2.5. Fuzzy Logic Technique

The advent of microcontrollers and Digital Signal Processors (DSPs) has made Fuzzy Logic Controllers (FLC) attractive in MPPT applications. This is because of their inherent advantages as follows: 1) having the ability to work on nonlinear systems, 2) not needing dynamic mathematical models, 3) ability to use imprecise inputs and 4) the ability to control unstable systems [25]. The basic structure of any FLC is shown in Figure 8, where the three major components are also

shown. The fuzzification stage converts the input variables into linguistic variables based on the membership functions. The fuzzy inference engine processes the inputs according to the rules set and produces the fuzzy outputs while the defuzzification stage produces the crisp real value for the fuzzy output [25]. For fuzzy logic-based MPPT controller, the error, equation (15), and the change of error, equation (16), are used as inputs to the fuzzifier because of the fact that at MPP, dP/dV approaches to zero [25].

$$E(n) = \frac{P(n) - P(n-1)}{V(n) - V(n-1)} \quad (15)$$

$$\Delta E(n) = E(n) - E(n-1) \quad (16)$$

The crisp input values of the error and change of error are then fuzzified into a set of fuzzy values by using appropriate membership functions. Based on the designed fuzzy rule base, the fuzzy inference engine derives a set of fuzzy results [26]. Finally, the output stage, which is the defuzzifier, combines and transforms the fuzzy results in crisp output value. The defuzzification process produces an analog output signal, a change in the duty ratio, which controls the power output of the MPPT system. Figure 9 shows the implementation of the FLC-based MPPT system of a PV power plant [25, 27].

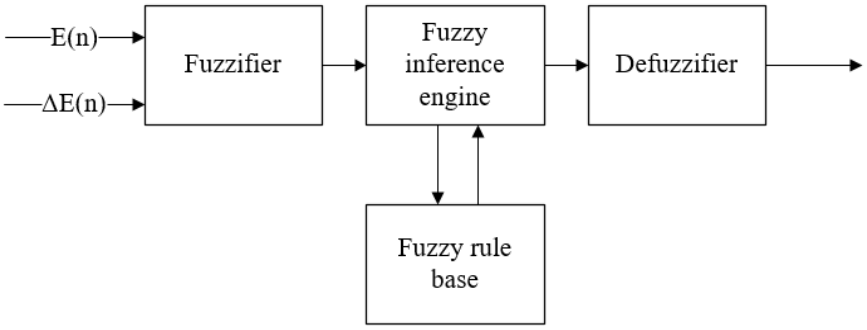

Fig. 8. Main components of a FLC.

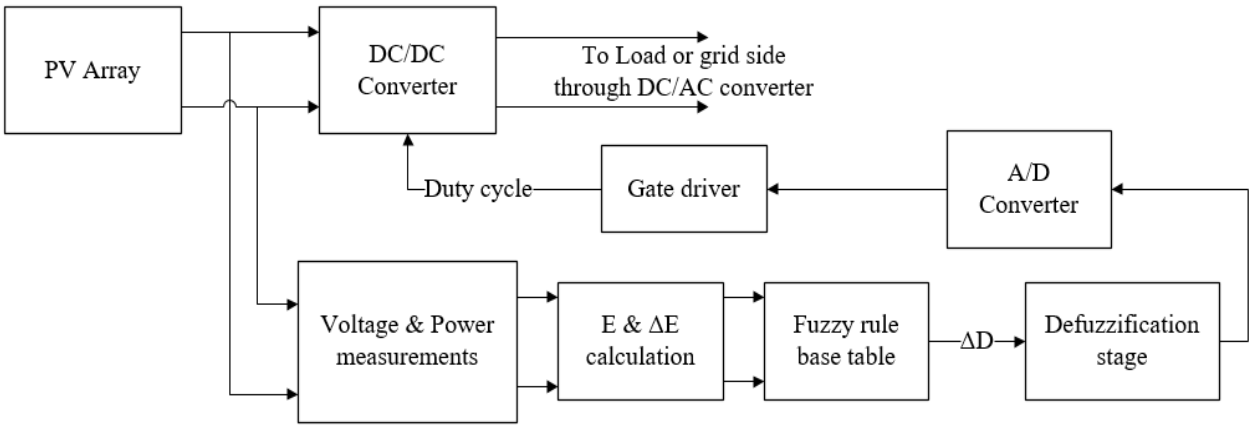

Fig. 9. Fuzzy logic controller-based MPPT implementation for a PV power plant.

The advantages of the FLC-based MPPT include [25-27]: 1) it has more flexibility and intelligence than conventional MPPT techniques; 2) effectively handles systems with nonlinearities and imprecise inputs; 3) good performance under varying weather conditions. It has the major disadvantage of requiring more memory space for implementation when compared to other MPPT techniques.

2.6. Fractional Open-Circuit Voltage-Based MPPT

This method is based on the fact that the voltage at the maximum power point (V_{mpp}) is proportional to the open-circuit voltage (V_{OC}), under varying irradiance and temperature conditions:

$$V_{mpp} = kV_{OC} \quad (17)$$

where k, is a constant which is dependent on the characteristics of the PV panel. This control technique requires measurement of the V_{OC} and V_{mpp} at different irradiance and temperature levels for the determination of the constant. Generally, this value is between 0.71 and 0.78 [8]. With the determined value of the constant, the voltage at the maximum power point is easily determined from equation (17). To overcome problems associated with the constant disconnection of the PV output terminals to take measurements of V_{OC}, pilot cells, which are exposed to the same environmental conditions are used. This technique has the advantages of ease of implementation because it does not require a complex control system and it is cheap to implement [8]. The disadvantages of the technique include [8, 9]: 1) temporary loss of power as a result of disconnection of PV array from the converter when taking measurements; 2) use of extra pilot cells for measurement; 3) unreliable performance under partial shading conditions.

3. REVIEW OF CLOSED LOOP CONTROL TECHNIQUES

To obtain a precise and well-regulated output voltage that is irresponsive to load changes and input voltage changes, a feedback technique is always used in modern switch-mode power converters [28]. For pulse-width modulation (PWM) based converters, while the early converters used only voltage-mode control technique, modern converters rely heavily on the use of the current-mode control technique [28]. The subsections below briefly explain the working principles of these two broad approaches to the control of power converters.

3.1. Voltage Mode Control

In this control approach, the output voltage regulated is sensed and fed back through an amplifier. For a PWM controlled converter, the feedback signal is then compared with a precision reference voltage [28, 30]. The comparator generates an error voltage (v_e), which is fed to the compensator network to generate the input to the pulse width modulator. The pulse width modulator, which is embedded, saw tooth reference signal (V_{cr}), then generates the switching pulses used to control the converter [30]:

$$D = \frac{v_e}{V_{cr}} \quad (18)$$

where, D is the duty cycle of the switching pulses. From equation (18), it is seen that when the output voltage is lower than the desired DC value (reference voltage), a higher error voltage is produced and consequently the duty cycle is increased to cause a subsequent increase in the output voltage. The opposite happens when the output voltage is higher than the reference voltage. Thus, by constantly controlling D, the output voltage is regulated [49]. The advantages of the voltage mode control are [30]: 1) ease of implementation and simplicity and, 2) good load regulation. The shortcomings of this method include [28, 29]: 1) slower line regulation reaction because changes in the input must first be translated into changes in output voltage and then fed back before corrective action is taken; 2) the slower response makes it unsuitable, when used alone, in PV applications that are characterized by fast dynamic changes.

3.2. Current Mode Control Technique

Current mode control is one of the most used control techniques employed in the control of switch-mode power converters. It relies on the use of current loop feedback in addition to the voltage loop. This multiple-loop approach to control uses either the inductor or switch current and the output voltage error signal as the control variables. The use of multiple control variables results in improved line and load transient response [24, 31]. These variables are used to generate inputs to the PWM modulator or gate pulses which are the final switching signals. Several variants of the current mode control exist in the literature [31-35]. A short review of some of the variants is presented in the subsections below.

3.2.1. Peak Current Control

While the conventional voltage-mode control has only one feedback loop with the output voltage as the control variable, the peak current control methodology utilizes the inductor current as an additional control variable, and thus achieves an improved input transient response [24, 31]. Figure 10 (a) shows a variant of the peak-current control method applied to a SEPIC converter. In the inner loop (green solid line enclosure), the resistor (R_C), senses the inductor current (i_L), to generate the voltage (v_c), which is the feedback control variable for this loop. The outer loop (blue solid line enclosure) uses the feedback control variable (v_e), which is the amplified error signal between the desired output voltage (V_{ref}) and the actual output voltage (V_o).

Figure 10 (b) depicts the waveforms involved in peak-current control and explains the operation. At the beginning of the switching cycle, the switch Q_1 is turned ON and the diode, D_1, turned OFF. Turning ON Q_1 causes the inductor current (i_L), and the associated voltage drop (v_c), across the sensing resistor to increase linearly from the initial value. When v_c increases to v_e, the amplified error signal from the outer loop of the voltage mode control, Q_1 is turned OFF and D_1 is turned ON. This makes i_L and v_c to decrease linearly until the end of the switching cycle. Thus, the meetings of the peak of v_c with v_e control the switching of Q_1 [34].

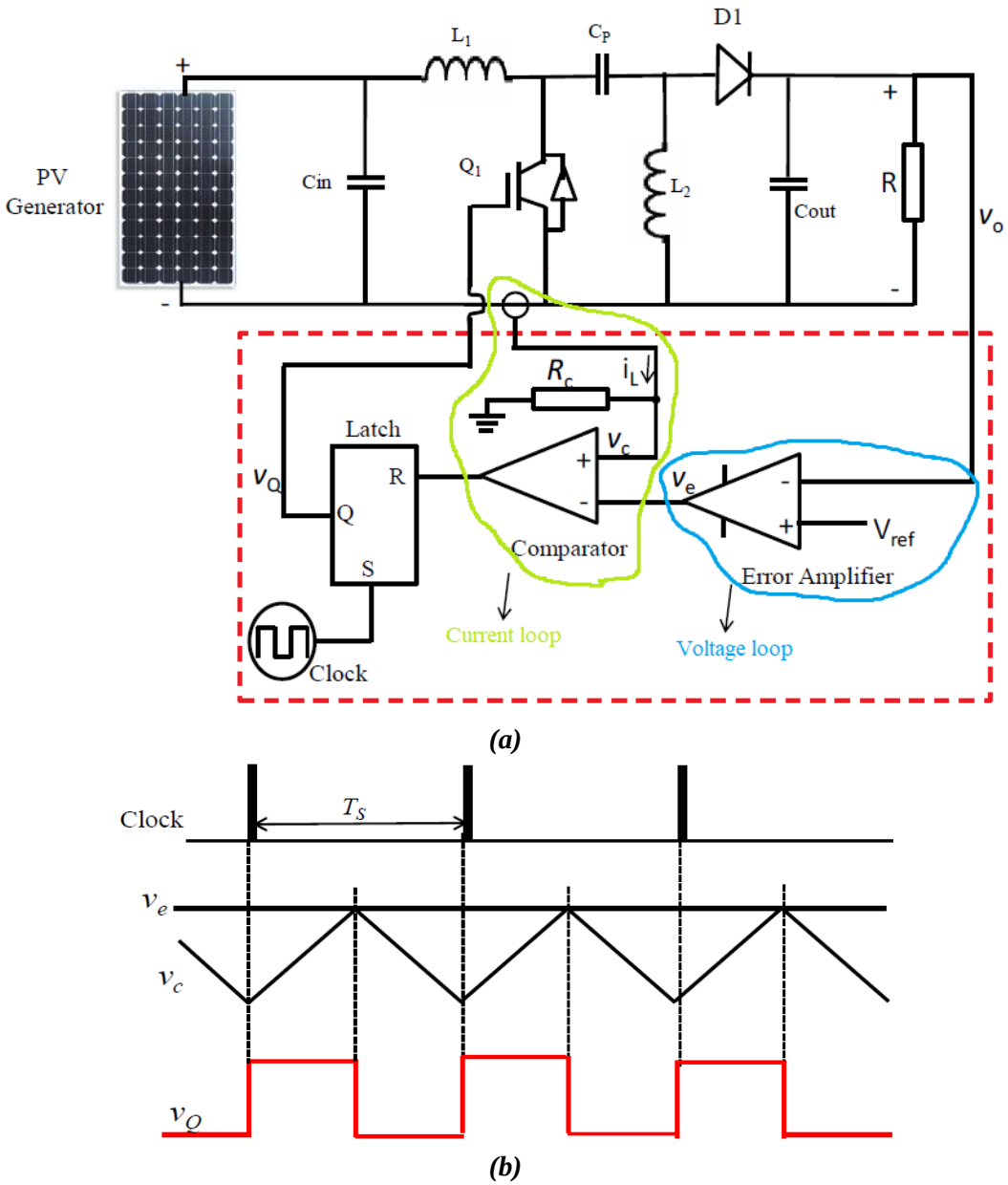

Fig. 10. Peak-current-controlled SEPIC converter. (a) Circuit. (b) CCM operation waveforms.

3.2.2. Average Current Control

This control scheme utilizes two cascaded loops that are dynamically separated, Figure 11. The inner current loop (blue solid line enclosure) is faster than the outer voltage loop (red solid line enclosure) [31]. Figure 11 explains the operation of this control methodology. It is seen from Figure 11 that the outer voltage loop (green solid line enclosure) compares the sensed output voltage (V_o), with the fixed reference voltage (V_{ref}). The difference, v_e, is amplified by the compensator (a proportional-plus-integral network) to generate K_{ve} as an error output. K_{ve} acts as a current reference for the inner current loop (red solid line enclosure), where

the sensed current is acquired via the sense resistor (R_S). The sensed voltage of R_S, V_{in}, is compared with K_{ve} to generate the output error (i_e), which is amplified and used for comparison in the pulse-width modulator to generate the gate switching pulses.

This mode of control has the following merits [31-33]: 1) faster transient response to load and input voltage changes when compared to voltage mode control or peak current mode control; 2) tracks the reference current with a high degree of accuracy; 3) slope compensation is not necessary; 4) it offers excellent noise immunity.

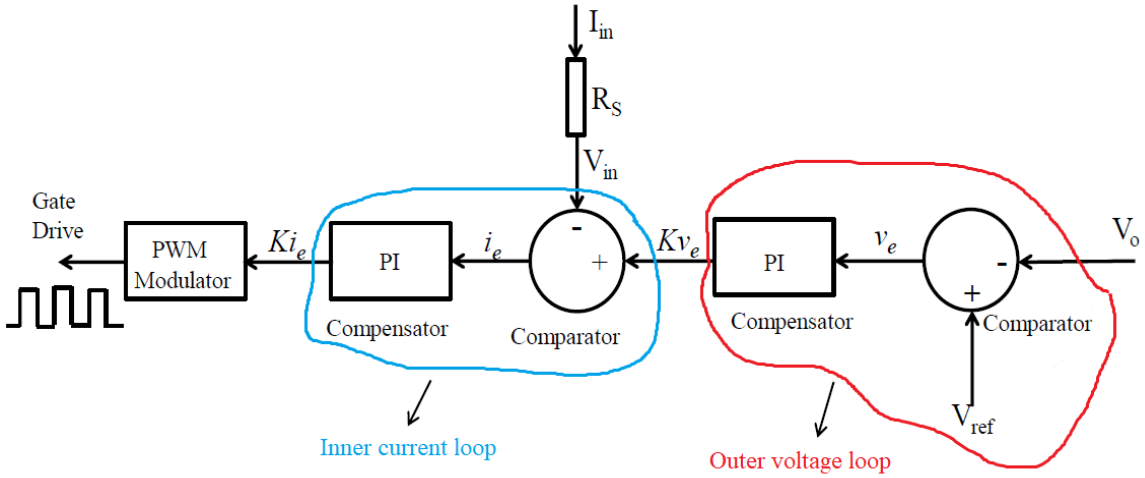

Fig. 11. Principle of operation of the average current control mode.

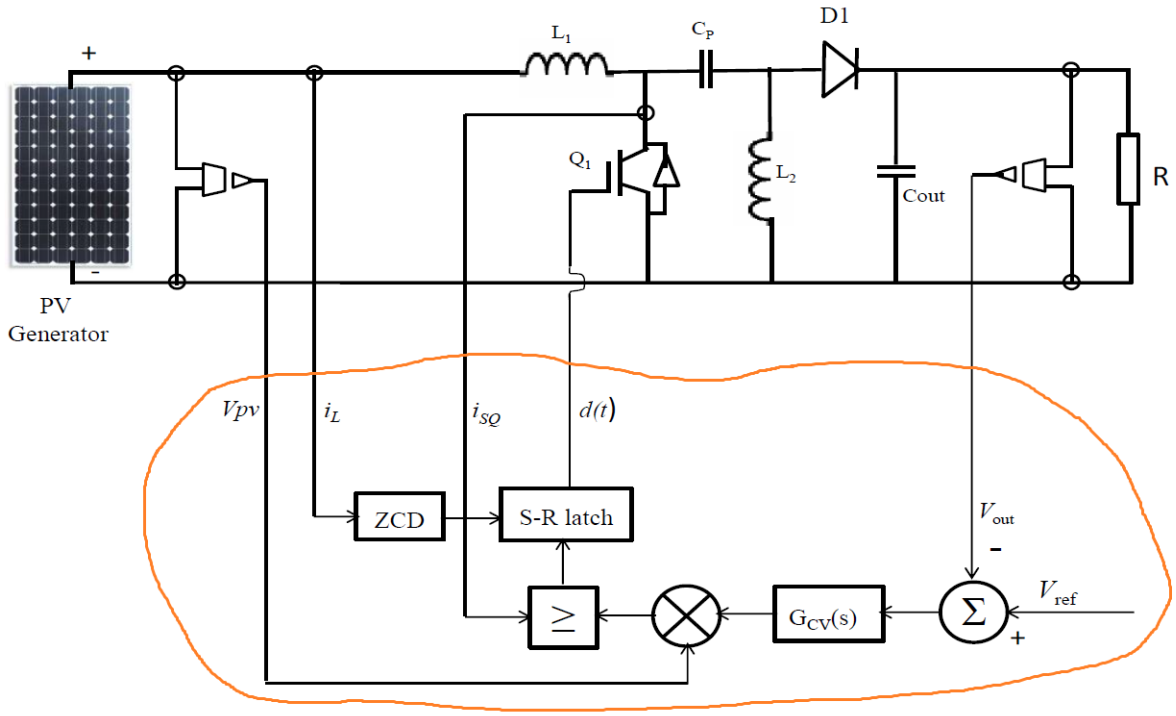

Fig. 12. SEPIC converter with hysteresis current control method.

3.2.3. Hysteresis Current Control

Hysteresis control is the control method in which the controlled variable, often the inductor current, is maintained between pre-set upper and lower limits [29]. The control scheme turns the switch OFF when the inductor current reaches the upper limit and turns it OFF when the current reaches the lower limit. Thus, the average inductor current is set at the average of the upper and lower thresholds. Figure 12 shows the hysteresis current control method applied to the SEPIC converter. The operation of the circuit is explained as follows [3]. The zero-current detector (ZCD) is used to sense the inductor current (i_L). Thus, the ZCD sets the SR-latch and turns ON the switch to initiate a switching cycle. In addition to the inductor current, the switch current (i_{SQ}), is also monitored and compared to a reference voltage that is proportional to the input voltage (V_{PV}). When equality is achieved between the sensed current and the reference, the latch is reset and the switch is turned OFF.

4. PROPOSED MULTI-LOOP MPPT AND CURRENT MODE CONTROL

4.1. An Improved I&C MPPT with Variable Step-Size Perturbation

As seen in Section 2.3, in the conventional I&C MPPT technique, a fixed, small iteration step size determined by accuracy and tracking speed requirement is used. With the use of such a fixed iteration step size, it is very difficult to achieve a rapid dynamic response and good steady-state accuracy simultaneously. If this step size increases, the tracking speed will also increase but with reduced tracking accuracy [14-17]. Conversely, if the step size is reduced, the tracking speed is reduced, but the tracking accuracy is increased. To overcome these limitations, this paper proposes an improved version of the I&C MPPT technique based on the application of variable step size for the perturbation. Compared to the conventional I&C technique which uses a fixed step size for perturbation, this improved algorithm simultaneously offers: 1) improved MPPT speed and, 2) improved MPPT accuracy.

In the proposed approach, the perturbation step-size, δV, is tuned automatically based on the PV array characteristics. When the operating point is far from the MPP, the step size will automatically increase and the tracking speed will increase consequently. Conversely, when the operating point is close to the MPP, the step size automatically decreases with the resultant decline of the steady-state oscillation. The flowchart of this MPPT approach is shown in Figure 13.

The step size is defined by:

$$\delta V = K \times \left|\frac{\Delta P}{\Delta V}\right| \tag{19}$$

where, K is the scaling factor.

4.2. Multi-Loop System for MPPT and Current Mode Control

A multi-loop, multi-objective control system is developed to achieve the following desired aims simultaneously:

- Tracking the maximum power point using the modified I&C technique introduced in the above section.

- Regulation of the output voltage of the SEPIC converter in the face of changes in the input or load.
- Controlling the inductor current.
- Ensuring the system's stability.

Figure 14 shows the block diagram of the multi-loop system. In this Figure, the MPPT block of Loop 1 (blue solid line enclosure), monitors the voltage and current at the terminals of the PV array and generates a reference voltage (V_{mpp}), which it uses to control the input voltage of the converter by forcing the PV array to operate at this voltage using the PI controller. The voltage controller of Loop 2 (green solid line enclosure), ensures the regulation of the output voltage of the converter while the innermost loop, Loop 3 (red solid line enclosure), ensures the control of the inductor current (i_L), using the average current mode control technique. The PWM block then produces the pulse train that operates the gate of the switch.

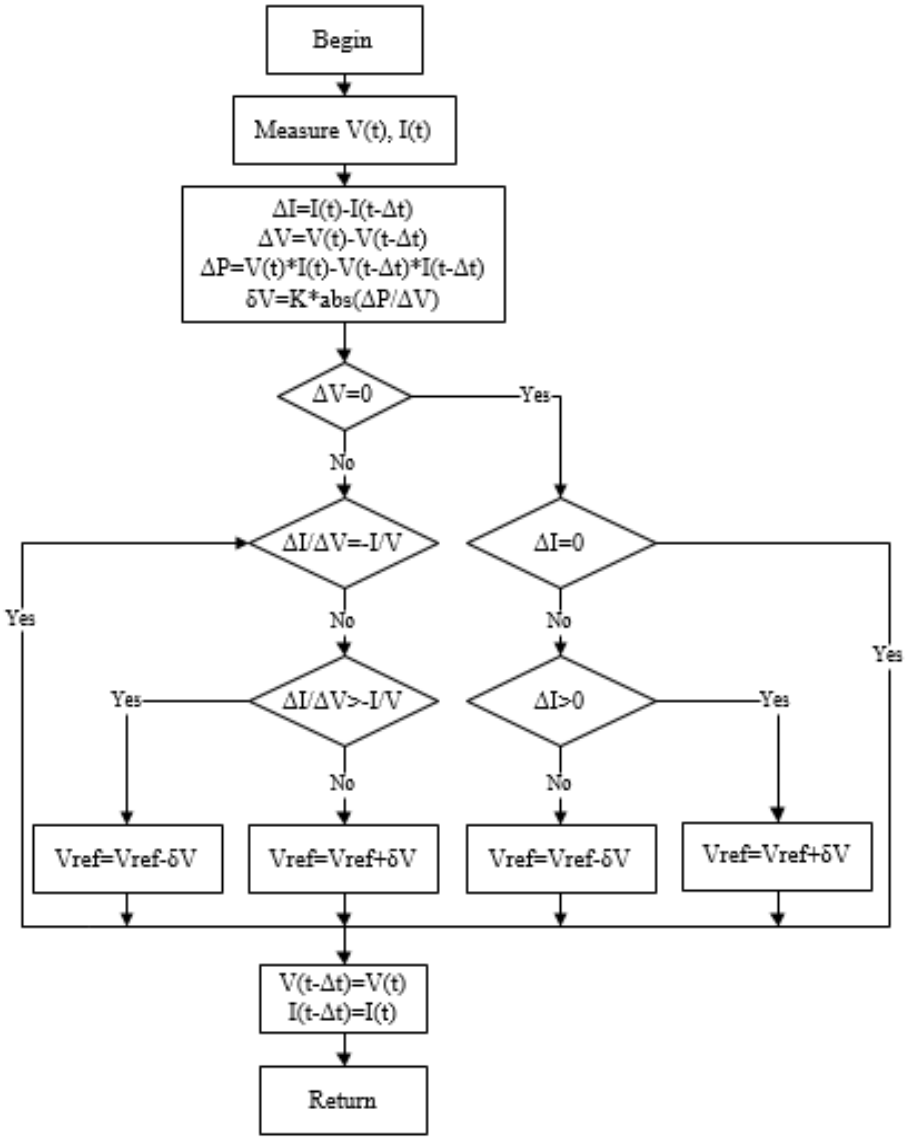

Fig. 13. Flowchart of the proposed variable step size I&C MPPT technique.

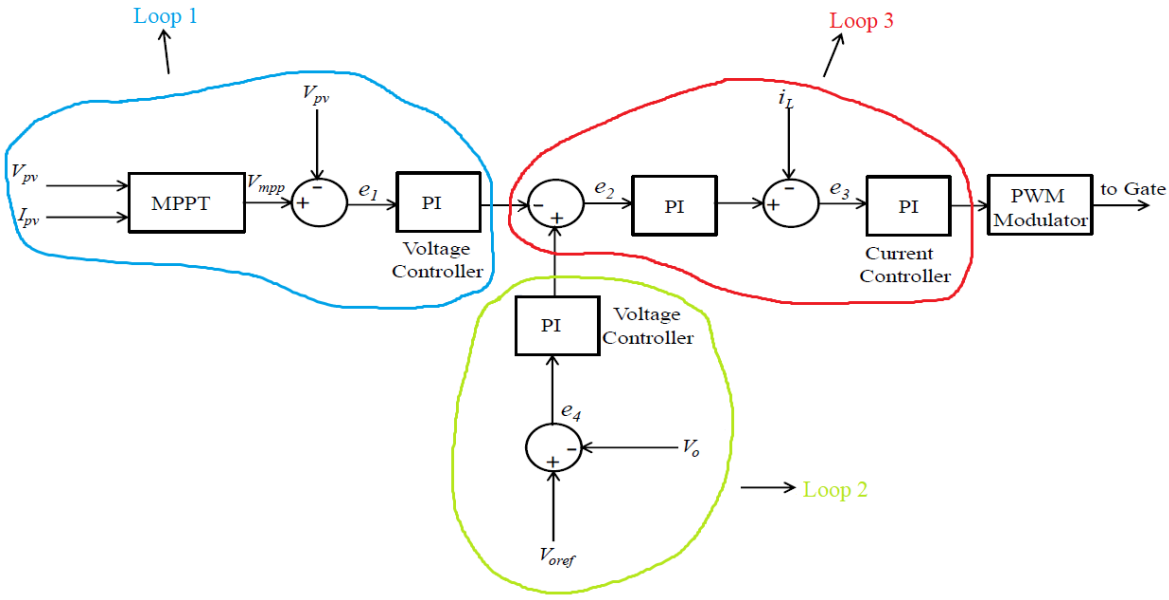

Fig. 14. Block diagram of the multi-loop system for MPPT and current mode control.

Table 1. ***Parameters of BP380 solar module at STC.***

Parameter	Value
Maximum power (P_{max})	80 W
Voltage at P_{max} (V_{mp})	17.6 V
Current at P_{max} (I_{mp})	4.55 A
Short-circuit current (I_{SC})	4.8 A
Open-circuit current (V_{OC})	22.1 V
Temperature coefficient of I_{SC} (alpha)	(0.065±0.015) %/℃
Temperature coefficient of V_{OC} (beta)	-(80±10) mV/℃
Temperature coefficient of power (gamma)	-(0.5±0.05) %/℃
Nominal Operating Cell Temperature (NOCT)	(47±2) ℃
Maximum system voltage	600 V

5. SIMULATION

A simulation model is developed using MATLAB/Simulink dynamic system simulation software to verify the operation of the control system developed in the previous section. The model takes solar irradiation and ambient temperature as inputs and generates PV module current and voltage, and consequently, module power as output.

Different parameters of the BP380 module used for the study such as the open-circuit voltage, short circuit current, voltage and current at the maximum power point and the temperature-based coefficients (alpha, beta, and gamma) can also be set in the model. The parameters of the BP380 solar module used are shown in Table 1.

The SEPIC converter is used as the DC-DC power conversion interface. The DC-DC converter is to generate the 180 *V* output and implement the MPPT of the PV module based on the tracking algorithm. The PV model uses the ambient temperature and insolation to generate the voltage, current and hence power, which characterizes the BP380 solar module used for the study. The produced power is processed by the SEPIC converter. For the implementation of the control strategy for the MPPT and current-mode operation, the PV module voltage, current, power, and the inductor current are continuously monitored.

To transfer the MPPT algorithm into the Simulink platform, the flowchart of Figure 13 is coded using the Embedded MATLAB function block of Simulink. This MPPT controller generates a reference voltage. This reference voltage, the inductor current, and the feedback voltage are used in the multi-loop feedback system. Figure 15 shows the simulation model for the MPPT with the integrated current mode control.

6. RESULTS AND DISCUSSION

The model, Figure 15, was simulated under different irradiance and ambient temperature conditions to study the effectiveness of the developed algorithm. The details are presented in the following subsections.

6.1. Effect of Irradiance Changes

To verify the performance of the improved MPPT technique with the current mode control, the PV system is simulated with a series of values of solar irradiance at constant ambient temperature. The simulation results,

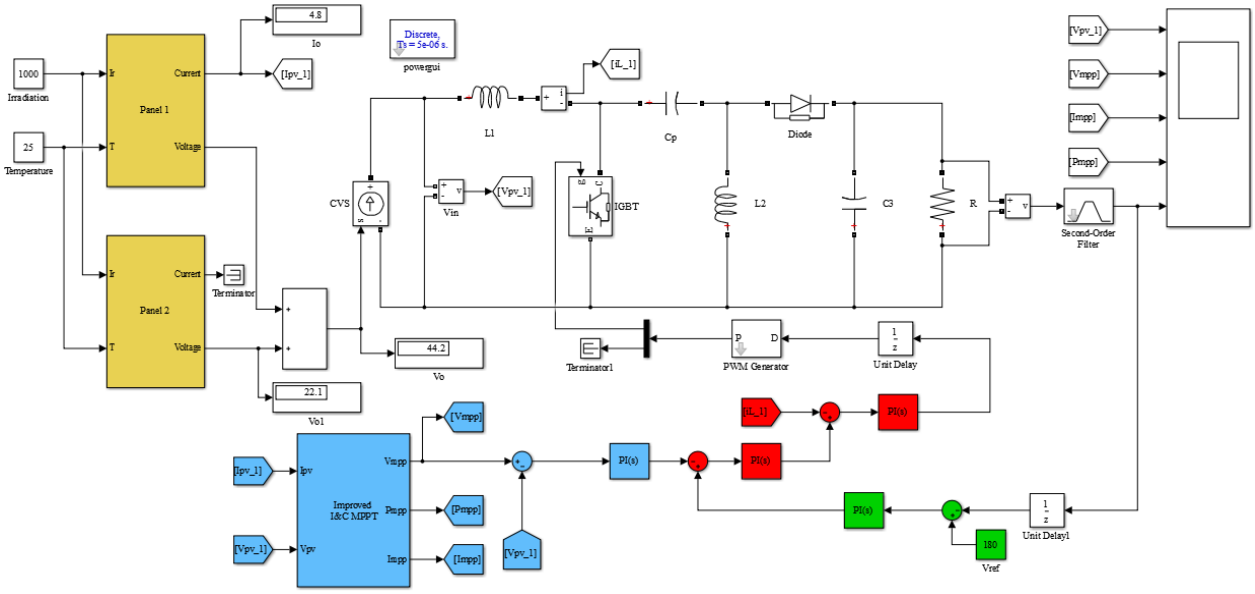

Fig. 15. Simulation model of the PV system with MPPT and current mode control in Simulink.

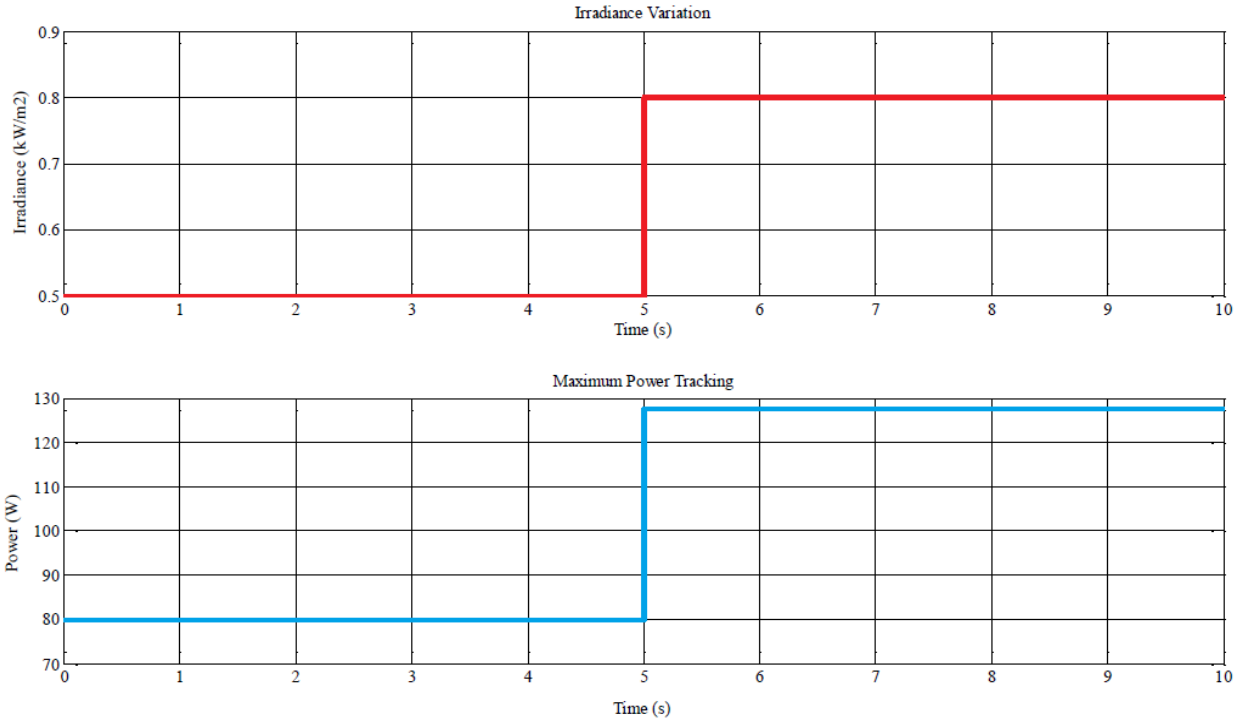

Fig. 16. Irradiation variation and MPPT at 25°C.

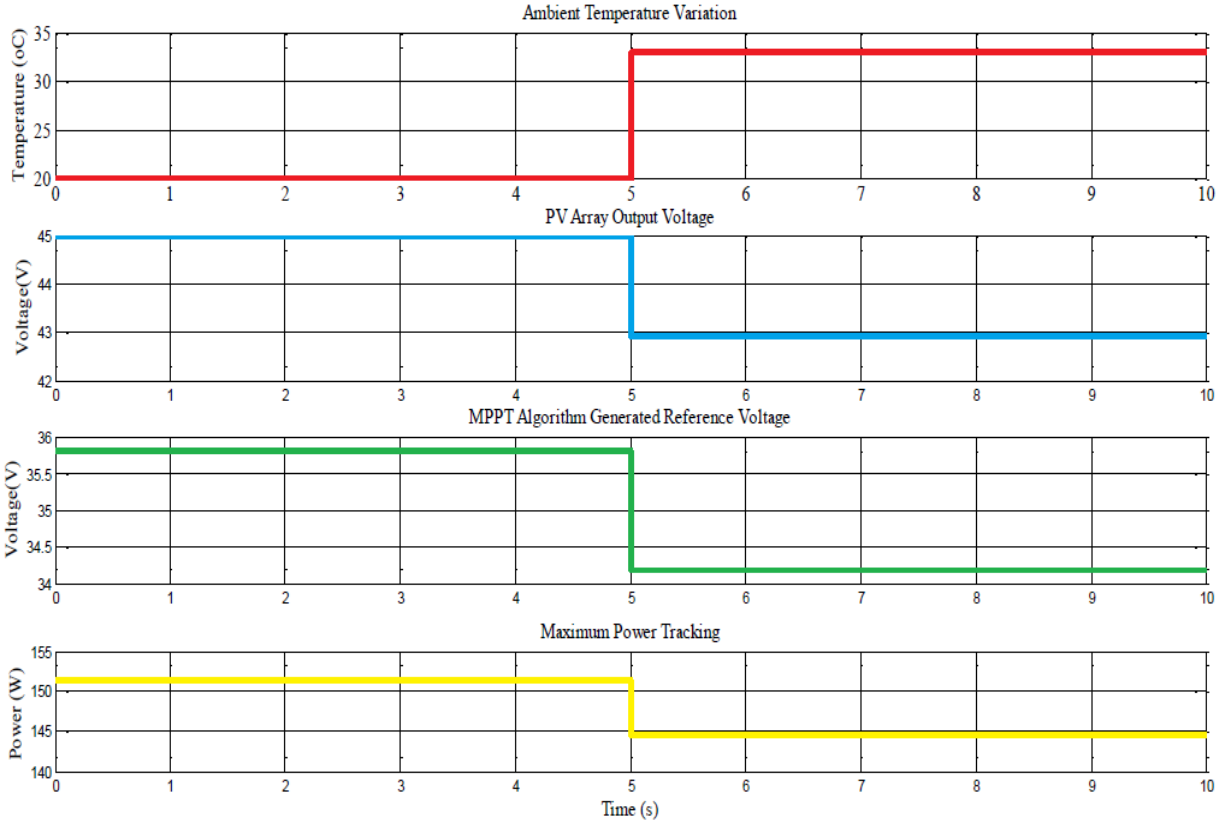

Fig. 17. Ambient temperature variation and MPPT performance.

Figure 16, show the solar irradiance changing abruptly from 500 W/m^2 to 800 W/m^2 at the step time of 5 seconds, when the ambient temperature is constant at 25 ℃. It is observed that the maximum power tracked changes correspondingly from 80 W to 128 W at the same step time of 5 seconds. The MPP changes rapidly with the same rapidity as the irradiance change and therefore ensures that optimum use of the PV array power is made.

6.2. Effect of Ambient Temperature Change

Figures 17 and 18 show the results of the simulation for varying ambient temperature at constant irradiance of 1000 W/m^2. In this system, the SEPIC converter input voltage is controlled to follow the reference voltage (V_{mpp}) determined by the improved I&C algorithm. Figure 17 shows the ambient temperature increasing abruptly from 20 ℃ to 33 ℃ at a step time of 5 seconds. For this increase, the PV array output voltage is seen to decrease from the initial value of 45 V to 42.9 V while the algorithm generated voltage drops from 35.8 V to 34.2 V at the same step time. Consequently, the tracked maximum power decreases from 152 V to 145 V at the same step time. The speed and accuracy of the tracking algorithm are obvious. Figure 18 also shows that despite the increase in ambient temperature from 20 ℃ to 33 ℃ and the attendant drop in the tracked power, the integrated current mode controller achieves a better regulation of the output voltage at the desired value of 180 V.

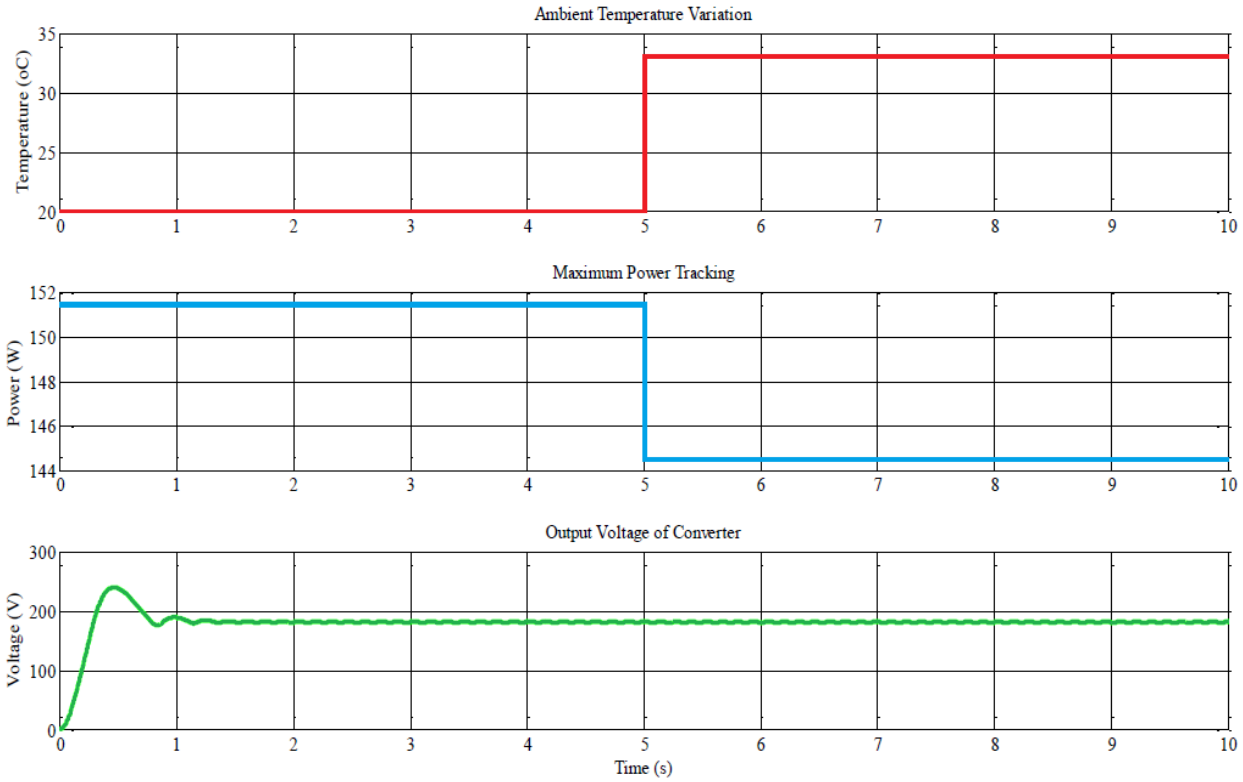

Fig. 18. Temperature variation, MPP and regulated output voltage of the converter.

7. CONCLUSION

This paper has reviewed the major existing MPPT techniques, highlighting the merits and the demerits of each approach. Similarly, the different approaches to current mode control have been reviewed. An improved MPPT technique based on the I&C technique has been proposed. The proposed technique with an integrated current mode control multi-loop system has been used to control the PV-SEPIC converter system. Accuracy and speed of response are the two main considerations in the implementation of any reliable MPPT algorithm since the changes in ambient temperature and solar irradiation are so unpredictable and happen so quickly. The results show that the developed multi-loop system can effectively track the MPP rapidly and accurately under different solar irradiance changes and alters in ambient temperature. Moreover, the system is seen to offer robust voltage regulation and improved dynamic response in the face of changing environmental variables.

REFERENCES

[1] M. Veerachary. Power Tracking for Nonlinear PV Sources with Coupled Inductor SEPIC Converter. IEEE Trans. Aerospace & Electronics Systems, vol. 40, no. 3, pp. 1019-1029, 2005.

[2] M. A. Danandeh, S. M. Mousavi G. Comparative and Comprehensive Review of Maximum Power Point Tracking Methods for PV Cells. Renewable and Sustainable Energy Reviews, vol. 82, no.3, pp. 2743-2767, 2018.

[3] K. N. Hasan. Control of Power Electronic Interfaces for Photovoltaic Power Systems. M.S thesis, Department of Electrical Engineering, University of Tasmania, Hobart, Australia 2009.

[4] S. Jianping, L. Xiaozheng. A New MPPT Control Strategy. Proc. Intl Conf. on Mechatronic Science, Electric Eng. & Computer (MEC), pp. 239-242, 2011.

[5] B. Liu, S. Duan, F. Liu, P. Xu. Analysis and Improvement of Maximum Power Point Tracking Algorithm Based on Incremental Conductance Method for Photovoltaic Array. Proc. 7th Intl Conf. on Power Electronics & Drives Systems, pp. 637-641, 2007.

[6] T. Esram, P. L. Chapman. Comparison of Photovoltaic Array Maximum Power Point Tracking Techniques. IEEE Trans. Energy Conversion, vol. 22, no. 2, pp. 439-449, 2007.

[7] M. K. Hossain, M. H. Ali. Overview on Maximum Power Point Tracking (MPPT) Techniques for Photovoltaic Power Systems. International Review of Electrical Engineering (IREE), vol. 8, no. 4, pp. 1363-1378, 2013.

[8] R. Faranda, S. Leva. Energy Comparison of MPPT Techniques for Photovoltaic Systems. WSEAS Trans. Power Systems, vol. 3, no. 6, 446-455, 2008.

[9] H. Cha, S. Lee. Design and Implementation of Photovoltaic Power Conditioning System Using a Current Based Maximum Power Point Tracking. Proc. IEEE Ind. Applications Society Annual Meeting, pp. 1-5, 2008.

[10] J. Olamaei, S. Ebrahimi, A. Moghassemi. Compensation of Voltage Sag Caused by Partial Shading in Grid-Connected PV System Through the Three-Level SVM Inverter. Sustainable Energy Technology & Assessments, vol. 18, pp. 107-118, 2016.

[11] M. G. Villalva, F. E. Ruppert. Analysis

and Simulation of the P&O MPPT Algorithm Using the Linearized PV Array Model. Proc. 35th Annual Conf. IEEE Industrial Electronics, pp. 231-236, 2009.

[12] N. Fermia, G. Petrone, G. Spagnuolo, M. Vitelli. Optimization of Perturb and Observe Maximum Power Point Tracking Method. IEEE Trans. Power Electronics, vol. 20, no. 4, pp. 963-973, 2005.

[13] N. Femia, D. Granozio, G. Petrone, G. Spagnuolo, M. Vitelli. Predictive and Adaptive MPPT Perturb and Observe Method. IEEE Trans. Aerospace & Electronic Systems, vol. 43, no. 3, pp. 934-950, 2007.

[14] El-Khozondar H. J., El-Khozondar R. J., Matter K., Suntio T. A Review Study of Photovoltaic Array Maximum Power Tracking Algorithms. Renewables: Wind, Water, and Solar, vol. 3, no. 3, 2016.

[15] W. Ping, D. Hui, D. Changyu, Q. Shengbiao. An Improved MPPT Algorithm Based on Traditional Incremental Conductance Method. Proc. 4th Intl Conf. on Power Electronics Systems & Applications (PESA), pp. 1-4, 2011.

[16] D. Menniti, A. Burgio, N. Sorrentino, A. Pinnarelli, G. Brusco. An Incremental Conductance Method with Variable Step Size for MPPT: Design and Implementation. Proc. 10th Intl Conf. on Electrical Power Quality & Utilisation, Lodz, Poland, pp. 1-5, 2009.

[17] Z. Yan, L. Fei, Y. Jinjun, D. Shanxu. Study on Realizing MPPT by Improved Incremental Conductance Method with Variable Step-Size. Proc. IEEE 3rd Conf. on Industrial Electronics & Applications, pp. 547-550, 2008.

[18] Y. Xiong, S. Qian, J. Xu. Research on Constant Voltage with Incremental Conductance MPPT Method. Proc. Asia-Pacific Power & Energy Engineering Conf. (APPEEC), pp. 1-4, 2012.

[19] J. Li, H. Wang. A Novel Stand-Alone PV Generation System Based on Variable Step Size INC MPPT and SVPWM Control. Proc. IEEE 6th Intl Conf. on Power Electronics & Motion Control, vol. 2155-2160, 2009.

[20] A. Safari, S. Mekhilef. Simulation and Hardware Implementation of Incremental Conductance MPPT with Direct Control Method Using Cuk Converter. IEEE Trans. Industrial Electronics, vol. 58, no. 4, pp. 1154-1161, 2011.

[21] T. Esram, J.W. Kimball, P. T. Krein, P.L. Chapman, P. Midya. Dynamic Maximum Power Point Tracking of Photovoltaic Arrays Using Ripple Correlation Control. IEEE Trans. Power Electronics, vol. 21, no. 5, pp.1282-1291, 2006.

[22] A. M. Bazzi, P. T. Krein. Ripple Correlation Control: An Extremum Seeking Control Perspective for Real-Time Optimization. IEEE Trans. Power Electronics, vol. 29, no. 2, pp. 988-995. 2014.

[23] J. W. Kimball, P.T. Krein. Digital Ripple Correlation Control for Photovoltaic Applications. Proc. Power Electronics Specialists Conf., pp. 1690-1694, 2007.

[24] G. Zhou, J. Xu, J. Wang. Constant-Frequency Peak-Ripple-Based Control of Buck Converter in CCM: Review, Unification, and Duality. IEEE Trans. Industrial Electronics, vol. 61, no. 3, pp. 1280-1291, 2014.

[25] Y. R. Yang. A Fuzzy Logic Controller for Maximum Power Point Tracking with 8-Bit Microcontroller. Proc. IEEE Industrial Electronics Society Annual Conference, pp. 2895-2900, 2010.

[26] S. Ozdemir, N. Altin, I. Sefa. Fuzzy Logic Based MPPT Controller for High Conversion Ratio Quadratic Boost Converter. International Journal of Hydrogen Energy, vol. 42, no. 28, pp. 17748-17759, 2017.

[27] C. Cecati, F. Ciancetta, P. Siano. A Multilevel Inverter for Photovoltaic Systems with Fuzzy Logic Control. IEEE Trans. Industrial Electronics, vol. 57, no. 12, pp. 4115-4125, 2010.

[28] M.H. Rashid. Power Electronics: Circuits, Devices, and Applications. 4th ed. Upper Saddle River, NJ, Pearson: USA; 2014.

[29] S. Winder. Power Supplies for LED Driving. 2nd ed. Elesevier: Oxford; 2008.

[30] K. Wu. Switch-Mode Power Converters: Design and Analysis. 1st ed. Elsevier: San Diego, USA; 2006.

[31] Y. Yan, F.C. Lee, P. Mattavelli, P. Liu. I^2 Average Current Mode Control for Switching Converters. IEEE Trans. Power Electronics, vol. 29, no. 4, pp. 2027-2036, 2014.

[32] Y. Yan, F.C. Lee, P. Mattavelli. Analysis and Design of Average Current Mode Control Using a Describing-Function-Based Equivalent Circuit Model. IEEE Trans. Power Electronics, vol. 28, no. 10, pp. 4732-4741, 2013.

[33] P. H. Liu, Y. Yan, F. C. Lee, P. Mattavelli. Universal Compensation Ramp Auto-Tuning Technique for Current Mode Controls of Switching Converters. IEEE Trans. Power Electronics, vol. 33, no. 2, pp. 970-974, 2018.

[34] B. Choi, W. Lim, S. Choi, J. Sun. Comparative Performance Evaluation of Current-Mode Control Schemes Adapted to Asymmetrically Driven Bridge-Type Pulse Width Modulated DC-DC Converters. IEEE Trans. Industrial Electronics, vol. 55, no. 5, pp. 2033-2042, 2008.

[35] C. Restrepo, T. Konjedic, J. Calvente, M. Milanovic, R. Giral. Fast Transitions Between Current Control Loops of the Coupled-Inductor Buck-Boost DC-DC Switching Converter. IEEE Trans. Power Electronics vol. 28, no. 8, pp. 3648-3652, 2013.